ARTICLE

Journal of Materials Chemistry
www.rsc.org/materials

Liquid-crystalline fullerene–ferrocene dyads

Stéphane Campidelli,[a] Ester Vázquez,[b] Dragana Milic,[b] Maurizio Prato,*[b] Joaquín Barberá,*[c] Dirk M. Guldi,*[d] Massimo Marcaccio,[e] Demis Paolucci,[e] Francesco Paolucci*[e] and Robert Deschenaux*[a]

[a]*Institut de Chimie, Université de Neuchâtel, Avenue de Bellevaux 51, Case postale 2, 2007 Neuchâtel, Switzerland. E-mail: robert.deschenaux@unine.ch*
[b]*Dipartimento di Scienze Farmaceutiche, Università di Trieste, Piazzale Europa 1, 34127 Trieste, Italy*
[c]*Química Orgánica, Facultad de Ciencias-Instituto de Ciencia de Materiales de Aragón, Universidad de Zaragoza-CSIC, 50009 Zaragoza, Spain*
[d]*University of Notre Dame, Radiation Laboratory, Notre Dame, Indiana 46556, USA*
[e]*Università di Bologna, Dipartimento di Chimica ''G. Ciamician'' via Selmi 2, 40126 Bologna, Italy*

Received 10th December 2003, Accepted 17th February 2004
First published as an Advance Article on the web 9th March 2004

The 1,3-dipolar cycloaddition reaction was used to assemble fullerene, ferrocene and a second-generation liquid-crystalline cyanobiphenyl-based dendrimer. The targeted compound displayed an enantiotropic smectic A phase from 40 to 135 °C. The *d*-layer spacing was determined by X-ray diffraction, and was found to be independent of temperature with a value of 95 Å. Molecular modeling and structural considerations suggested partial bilayer organization of the mesogenic molecular units within the smectic layers. Oxidation or reduction processes of the basic components (ferrocene, fullerene, dendrimer) were investigated by electrochemical techniques, and were in agreement with the structure. Photoinduced electron transfer from ferrocene to fullerene was identified, most likely with a ''through space'' mechanism.

Introduction

The design and study of functionalized molecular assemblies containing [60]fullerene (C_{60}) as an electron acceptor unit and various electron donor moieties (*e.g.* ferrocene,[1] TTF,[2] porphyrins,[3–5] carotenoids,[6] OPV[7–10]) has attracted considerable attention. Of particular interest are the possible applications of such materials in solar cell technology[7–13] and as optical- and/or redox-active molecular dyads, triads, or tetrads.[3–5,14]

Guldi *et al.*[15] described photoinduced electron transfer in a series of fulleropyrrolidines containing ferrocene (Fc) as electron donor. Depending on the nature of the bridge which connected the Fc and C_{60} units, two different mechanisms (through bond or space) for the migration of the electron from Fc to C_{60} were suggested.

Recently, we reported a liquid-crystalline fullerene–ferrocene dyad.[16,17] This compound was obtained by addition of a ferrocene-based mesomorphic malonate (containing cholesterol as liquid-crystalline promoter) to C_{60} by applying the Bingel reaction.[18,19] The Fc was included in the liquid-crystalline promoter. Both the malonate and the fullerene–ferrocene derivatives displayed smectic A phases. Photoinduced electron transfer with lifetimes of several hundred of nanoseconds was observed.[17]

To develop fullerene–ferrocene liquid-crystalline dyads with longer lifetimes of the charge separated state, and establish a structure–property relationship, we designed a material in which Fc is located at the end of a flexible chain, and which acts independently of the mesomorphic fragment. Such a structure is of interest as the redox potential of the Fc can be controlled with the degree of substitution, and the mesogenic properties can be tuned from the choice of the liquid-crystalline groups since Fc does not interfere with the mesomorphic moiety (as in our former prototype[16,17]).

Herein, we report the synthesis, liquid-crystalline properties, supramolecular organization, electrochemical and photophysical behavior of **1** (Scheme 1). Compared to our former investigations,[17] longer lifetimes for the charge separated state are obtained. This result is an indication that the substitution of the Fc unit and its location within the molecular architecture influence markedly the physical properties of the dyad.

Results and discussion

Synthesis

The synthesis of **1** is presented in Scheme 1. Addition of aldehyde **2**[20] and *N*-substituted glycine **3**[21] to C_{60} led to protected fulleropyrrolidine **4**. Removal of the Boc-protecting group under acidic conditions gave **5**. Finally, condensation of ferrocenecarboxylic acid with **5** furnished **1**. The purity of the compounds was confirmed by ^{1}H and ^{13}C NMR spectroscopy.

Liquid-crystalline properties

The thermal and liquid-crystalline properties of **1** and **2** were investigated by polarized optical microscopy (POM) and differential scanning calorimetry (DSC). The mesomorphic behavior of **1** was also analyzed by X-ray diffraction (XRD). The phase transition temperatures and enthalpies are reported in Table 1.

Compounds **1** and **2** showed smectic A phases which were identified by POM from the observation of focal-conic and homeotropic textures. Glass transition and isotropization temperatures were determined for **1** and **2** by DSC. Fullerene derivative **1** showed a lower clearing point than **2**. This behavior is in agreement with results obtained for other fullerene-containing liquid crystals,[22] and is due to the presence of Fc and C_{60}. Such bulky moieties alter the intermolecular interactions between the mesogenic units compared to their

DOI: 10.1039/b316085h

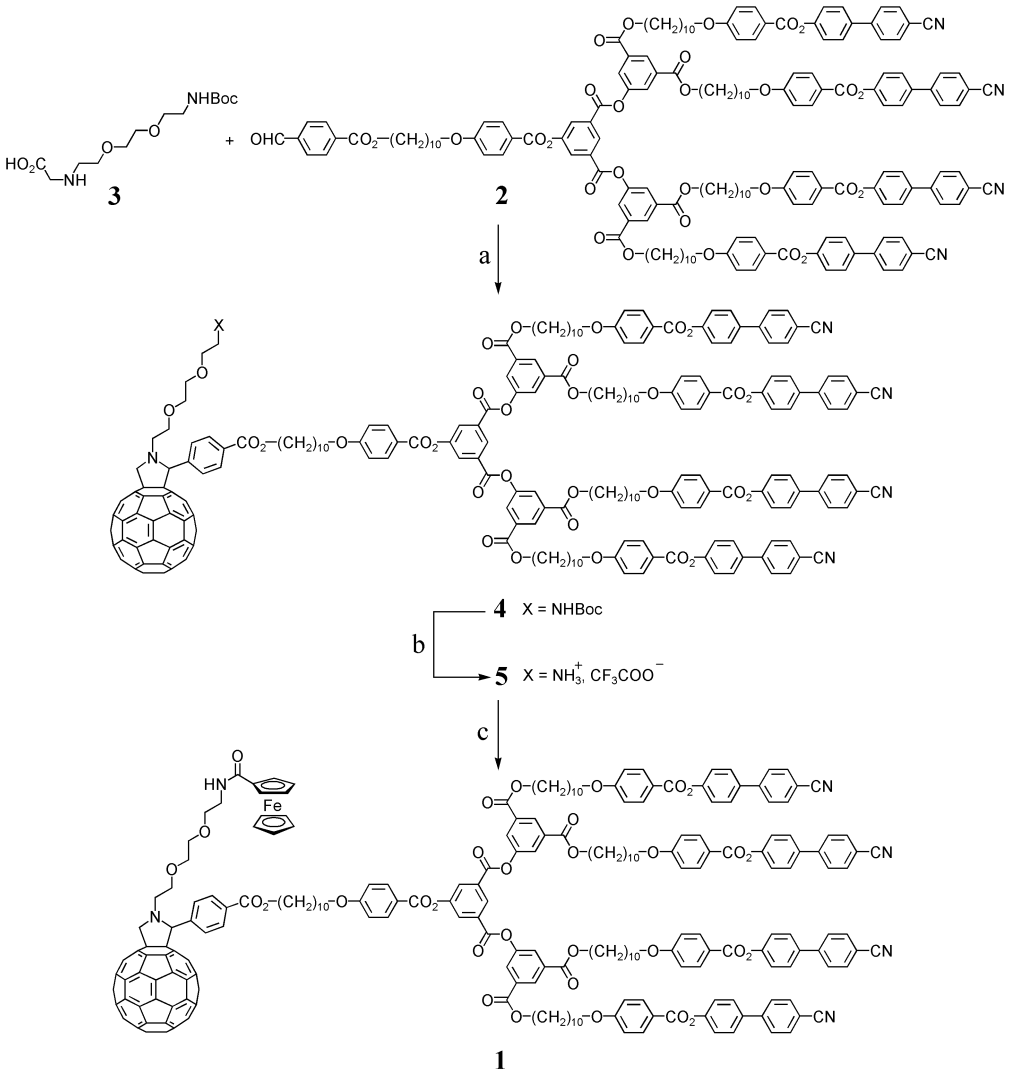

Scheme 1 a) C_{60}, toluene, reflux, 1 h, 79%. b) Trifluoroacetic acid (TFA), CH_2Cl_2, rt, 1 h, 95%. c) Ferrocenecarboxylic acid, Et_3N, 1-hydroxybenzotriazole (HOBT), 1-(3-dimethylaminopropyl)-3-ethylcarbodiimide hydrochloride (EDC), CH_2Cl_2, rt, overnight, 39%.

Table 1 Phase-transition temperatures[a] of **1** and **2**

Compound	Tg/°C	$S_A \rightarrow I$/°C	ΔH/kJ mol^{-1}
2	35	185	12.8
1	40	135[b]	12.9

[a] Tg = glass transition temperature, S_A = smectic A phase, I = isotropic liquid. Temperatures are given as the onset of the peak obtained during the second heating run; the Tg were determined during the first cooling. [b] Determined as the maximum of the peak during the first cooling run.

precursor **2**. When the samples were examined by POM, higher viscosity was observed for **1** than for **2**.

The smectic A phase of **1** was characterized by XRD at room temperature and from room temperature to 140 °C. In all cases, the patterns were consistent with the smectic A nature of the mesophase, except the pattern recorded at 140 °C which was characteristic of the isotropic liquid. A set of two equally-spaced maxima were found at small angles, which are characteristic of the reflection of the X-ray beam on the smectic layers. In the wide-angle region, only diffuse scattering was detected corresponding to the liquid-like arrangement of the mesogenic groups. The *d*-layer spacing was found to be independent of temperature. A value of about 95 Å was determined. When the sample was analyzed at room temperature, a diffraction pattern similar to those recorded above 40 °C was obtained, indicating that the sample did not crystallize upon cooling but gave rise to an anisotropic glass. This behavior is due to the dendritic core which prevents crystallization of the sample.

Supramolecular organization

To describe the supramolecular organization of **1** within the smectic A layers, it is necessary to take into account the cross-sectional areas of the C_{60} and mesogenic units as well as the interactions which occur from such a structure (attractions between the C_{60} units; dipolar interactions through the terminal dipole moments of the mesogenic groups; the natural tendency of the mesogenic groups to form an anisotropic organization within micro-domains).[23]

The molecular length (L) of **1** was estimated in its fully extended conformation obtained by means of HyperChem software, and was found to be about 68 Å. The d/L ratio of 1.4 reveals that **1** organizes into a partial bilayer smectic structure, in which the cyanobiphenyl groups are interdigitated from layer to layer. The adequacy between the cross-sectional areas of four mesogenic units (the cross-sectional area of one cyanobiphenyl group is about 22–25 Å^2) and of the fullerene moiety (about 90–100 Å^2) strengthens this model which was proposed for liquid-crystalline methanofullerenes also containing four cyanobiphenyl groups.[23] The Fc moieties should be localized between the C_{60} units and the dendritic cores. Furthermore, the C_{60} moieties of adjacent layers are located

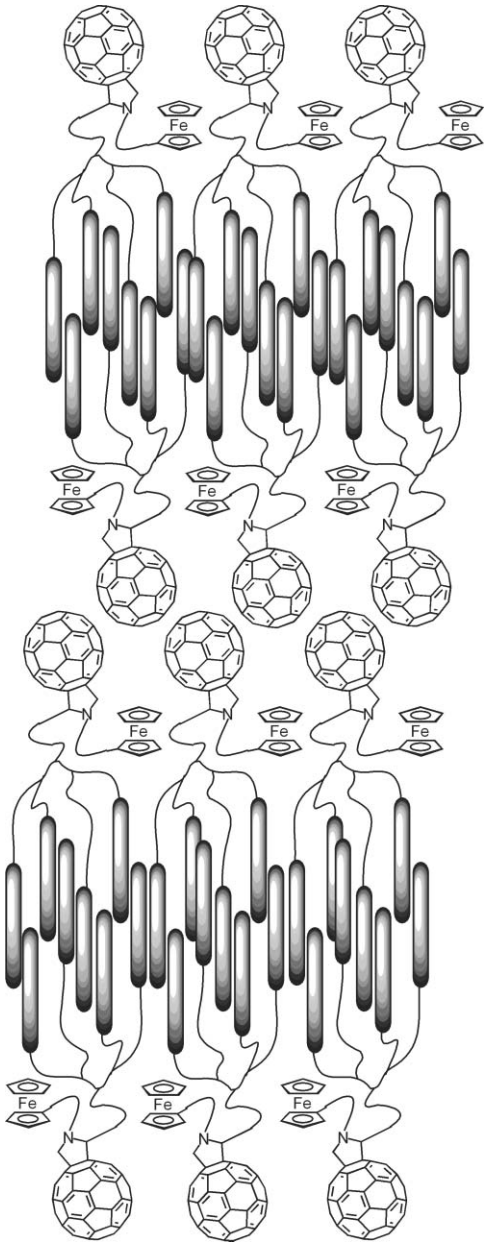

Fig. 1 Postulated supramolecular organization of **1** in the smectic layers.

side-by-side, giving rise to a superstructure with alternating sublayers containing either the mesogenic groups or the C_{60} units, respectively. This micro-segregated organization is the consequence of a combination of efficient space filling and strong interactions within each microdomain. The postulated supramolecular organization of **1** within the smectic A phase is presented in Fig. 1.

Electrochemistry

The cyclic voltammetric (CV) behavior of **1**, reference compound **6**[20] (Fig. 2) and dendrimer **2** was investigated in THF solution under strictly aprotic conditions.[24,25] Fig. 3a displays the CV curve of a 0.5 mM **1** THF solution, at 25 °C and scan rate 1 V s^{-1}. The anodic peak A, with $E_{1/2} = 0.70$ V, is attributed to the reversible one-electron oxidation of the ferrocene moiety, while peaks I, II and III ($E_{1/2} = -0.46$, -1.04 and -1.65 V) are associated with the reversible subsequent one-electron reductions of the fulleropyrrolidine.[26] Note that peak III displays a larger peak height than peaks A, I and II, indicating the occurrence of a further reduction process at a potential close to the third fullerene-centered reduction. Such a process involves the dendritic moiety in **1** (compare with Fig. 3c). At more negative potentials, an intense multielectron reduction peak (IV) is observed, associated with the occurrence of several reduction processes at close potentials. The fourth reduction of the fulleropyrrolidine moiety is known to occur at such potentials (*N*-methylfulleropyrrolidine undergoes a fourth reduction at -2.16 V[26]), while the remaining reduction processes are attributed to the dendritic moiety in **1**. As expected, the CV curve of **6** (Fig. 3b) displays the same redox pattern as **1**, except for the ferrocene-centered oxidation processes at 0.70 V. At potentials $\leqslant -2.3$ V, a further multielectron reduction peak (V) is observed which is similarly attributed to the dendritic moiety. Such a peak is, in fact, also observed for **2** (Fig. 3c) and **1** (not shown in Fig. 3a). Analysis of the CV curve of **2** (Fig. 3c) by convolution techniques[27] allowed evaluation of the number of electrons (n) associated with the subsequent reduction peaks involving the dendritic moiety: n(I) = 1, n(II) = 4, n(III) = 1, n(IV) = 3. Peak III (at about -2.30 V in Fig. 3c) is not observed in the CV curves of **1** and **6** and should involve the aromatic aldehyde terminal group in **2**. On the basis of the above n values and of the occurrence of the various electroactive groups within the dendritic structure, peak II in Fig. 3c was attributed to the reduction of the four equivalent cyanobiphenyl groups, while the processes comprising peak IV are likely to involve the three equivalent isophthaloyl ester moieties in the dendritic core. Finally, the reduction peak I might involve the benzoic ester moiety which is linked to the dendritic core.

Photophysical properties

Relative to reference compound **6**, which shows solvent-independent fluorescence quantum yields (6.0×10^{-4}),[1] the fullerene fluorescence (1.76 eV) in **1** is quenched by $\sim$50% (Table 2 and Fig. 4). We tested toluene, THF and benzonitrile (solvents of increasing polarity) to tune the energy gap for photoinduced electron transfer, which is one of the likely deactivation pathways in photoexcited **1**. On the basis of the electrochemical study, the charge-separated state, comprising an oxidized ferrocene and a reduced fulleropyrrolidine, would, in fact, lie at 0.84 eV in THF (0.72 eV in benzonitrile: a detailed description of the determination of the thermodynamic driving

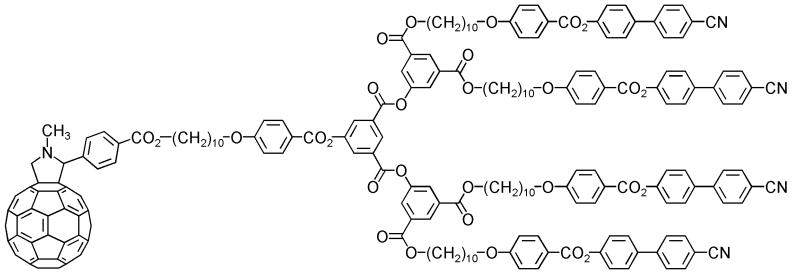

6

Fig. 2 Structure of reference compound **6**.

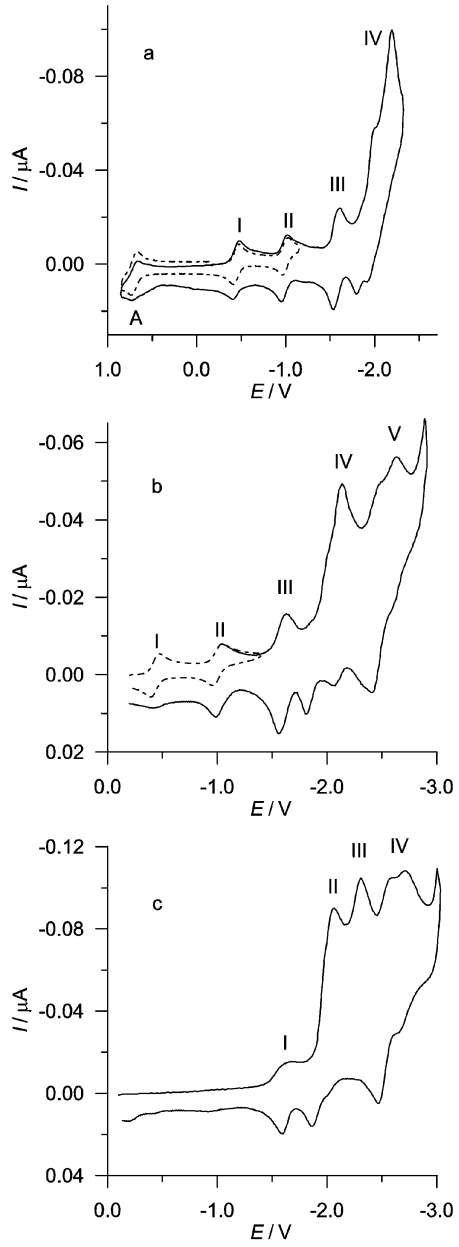

Fig. 3 CV curves of **1** (0.5 mM) (a), **6** (0.5 mM) (b) and **2** (0.5 mM) (c) in THF (0.05 M TBAH), at 25 °C and scan rate 1 V s^{-1}.

forces can be found in the footnote to Table 3), above ground state. Alternatively, a singlet–triplet energy transduction may occur, while a singlet–singlet energy transfer is ruled out on thermodynamic grounds (*i.e.*, uphill by 0.7 eV). The thermodynamic consequence on the electron transfer mechanism can be understood on the basis that radical ion pairs experience better solvation in polar environments, and that this results in lower energies of the resulting charge-separated state. It is important to note that the energy of the excited state (1.76 eV) remains unaffected. Only a moderate red-shift of about 5 nm is discernible on going from toluene to benzonitrile. Interestingly, the fullerene fluorescence quantum yields in **1** are virtually identical, despite the overall quenching and the variation in solvent polarity.[28]

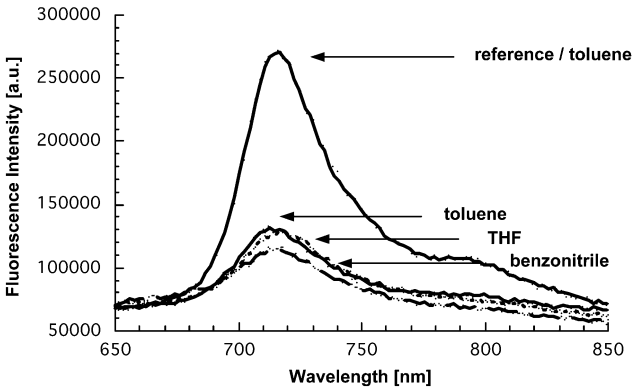

Fig. 4 Emission spectra of **6** in toluene (solid line) and **1** in different solvents with matching absorption at the 350 nm excitation wavelength. $OD_{310\ nm} = 0.5$.

Table 3 Driving force dependence (ΔG_S, $-\Delta G_{CR}^{\circ}$, $-\Delta G_{CS}^{\circ}$) for intramolecular electron transfer events in liquid crystal **1**

Solvent	ΔG_S[a]/eV	$-\Delta G_{CR}^{\circ}$[b]/eV	$-\Delta G_{CS}^{\circ}$[c]/eV
toluene	+0.09	1.25	0.51
THF	−0.32	0.84	0.92
PhCN	−0.45	0.71	1.05

[a] Determined from the following relations:

$$\Delta G_S = \frac{e^2}{4\pi\varepsilon_0}\left[\left(\frac{1}{2R_+}+\frac{1}{2R_-}-\frac{1}{R_{D-A}}\right)\frac{1}{\varepsilon_S}-\left(\frac{1}{2R_+}+\frac{1}{2R_-}\right)\frac{1}{\varepsilon_R}\right]$$

$E_{1/2}(D^{\bullet+}/D)$ = oxidation potential of donor (0.7 V *versus* SCE in THF); $E_{1/2}(A/A^{\bullet-})$ = reduction potential of acceptor (−0.46 V *versus* SCE in THF); R_+ = radius donor (3.7 Å); R_- = radius acceptor (4.4 Å); R_{D-A} = donor–acceptor separation (6.406 Å); ε_s = solvent dielectric constant (toluene = 2.39; THF = 7.6; benzonitrile = 24.8); ε_R = solvent dielectric constant for electrochemical measurements (7.6). [b] Determined from the following relation: $-\Delta G_{CR}^{\circ} = E_{1/2}(D^{\bullet+}/D) - E_{1/2}(A/A^{\bullet-}) + \Delta G_S$. [c] Determined from the following relation: $-\Delta G_{CS}^{\circ} = \Delta E_{0-0} - (-\Delta G_{CR})$; ΔE_{0-0} = excited state energy of the chromophore (1.76 eV).

Parallel to the steady-state experiments, we measured the fluorescence lifetimes in **6** and in **1** with a strobe system (*i.e.*, excitation wavelength: 337 nm). In comparison with the steady-state experiments, a qualitatively similar picture evolves. Firstly, **6** shows a solvent-independent lifetime of 1.8 ns (Fig. 5). Secondly, despite the energetic difference in the driving force, kinetic differences are hardly seen for **1**. The lifetimes are reduced by ~60%, and range between 0.79 and 0.84 ns (Table 2). Finally, no spectral evidence for new features such as charge-transfer is observed.

At this point, we would like to correlate the fluorescence data with structural aspects of **1**. It is important to realize that a flexible polyethyleneglycol chain links C_{60} with Fc, which gives room for configurational changes in the donor–acceptor structure, either in the ground state or once photoexcited.[15,29,30] Consequently, we should assume that the charge-separation process is mediated by "through-space" interactions between C_{60} and Fc.

The final set of experiments is concerned with transient absorption measurements. Upon pumping light into the ground state of **6** with a short 355 nm laser pulse, fullerene singlet–singlet features are registered with a maximum at

Table 2 Photophysical properties of **1**

	Fluorescence quantum yields (Φ)	Fluorescence decay (τ)/ns	Singlet decay (τ)/ns	Radical pair quantum yield (Φ)	Radical pair decay (τ)/ns
toluene	2.9×10^{-4}	0.79	0.82		
THF	2.8×10^{-4}	0.84	0.77	0.15	560
PhCN	2.9×10^{-4}	0.82	0.84	0.15	490

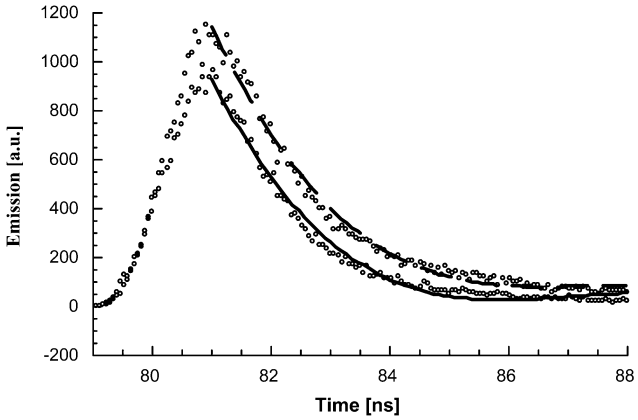

Fig. 5 Fluorescence decay profiles of **6** ($\sim 5.0 \times 10^{-5}$) in deoxygenated toluene (dashed line) and **1** in deoxygenated THF (solid line).

900 nm. Fig. 6 displays the singlet excited state features recorded with a 20 ps time delay. The lifetime of this intermediate state is relatively short, since, once formed, the lowest vibrational state of the singlet excited state undergoes rapid and quantitative intersystem crossing (ISC) to the energetically lower lying triplet. In **6**, crossing between the two manifolds takes place with a time constant of $7.4 \times 10^8\ s^{-1}$. Two maxima located at 360 and 700 nm and a low-energy shoulder around 800 nm characterize the fullerene triplet excited state. The transient absorption spectrum in Fig. 6, which is recorded with a 5000 ps time delay, exemplifies the 700 nm maximum and the 800 nm shoulder.

Transient absorption changes, recorded upon 355 nm laser excitation of **1**, reveal the same broad maximum, which was seen for **6** around 900 nm (similar to the 20 ps time component shown in Fig. 6). Time profiles, taken at various wavelengths, indicate that the fullerene singlet excited state is formed instantaneously and in a single step, but decays faster than in **6**. Again, the decay dynamics (ranging between 0.77 and 0.84 ns) are solvent-independent. More important is that the absorption, recorded after the conclusion of the fast singlet decay, is distinctly different from the triplet features (*i.e.*, maxima at 360 and 700 nm), as depicted in Fig. 7. In particular, a new maximum at 1000 nm,[1] which is persistent up to several hundred nanoseconds, resembles the fingerprint of the one-electron reduced form of fulleropyrrolidines.[1]

The radical anion fingerprint allowed us to determine the lifetime of the charge-separated state. The decay curves were well fitted by a single exponential decay component with

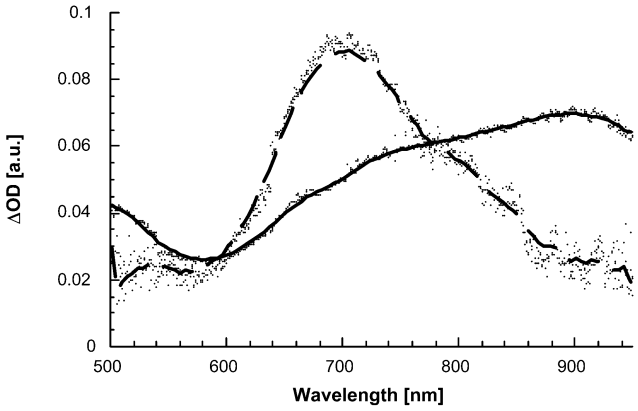

Fig. 6 Differential absorption spectra (visible and near-infrared) obtained upon picosecond flash photolysis (355 nm) of $\sim 1.0 \times 10^{-5}$ M solutions of **6** in nitrogen saturated toluene with a time delay of 20 ps (solid spectrum) and 5000 ps (dashed spectrum), showing the singlet and triplet excited state features of the photoexcited fullerene.

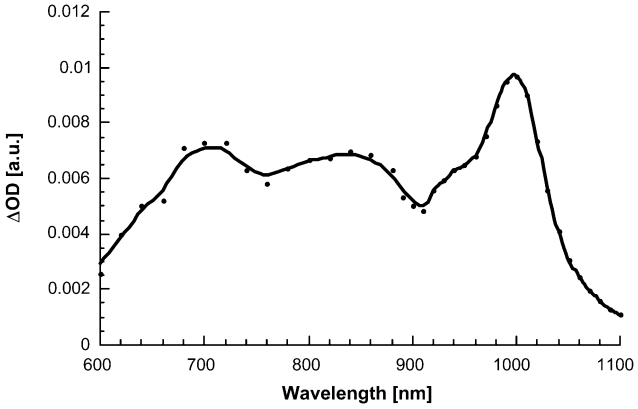

Fig. 7 Differential absorption spectrum (visible and near-infrared) obtained upon nanosecond flash photolysis (337 nm) of $\sim 1.0 \times 10^{-5}$ M solutions of **1** in nitrogen saturated THF with a time delay of 50 ns at room temperature.

lifetimes that are on the order of 560 ns (THF) and 490 ns (benzonitrile).

Conclusion

To develop liquid-crystalline dyads, fullerene, ferrocene and a second-generation mesomorphic dendrimer were assembled by applying the 1,3-dipolar cycloaddition reaction. The targeted compound displayed an enantiotropic smectic A phase, and organized into a partial bilayer structure. Electrochemical investigations showed oxidation or reduction processes associated with ferrocene, fullerene and the dendritic moiety. Photoinduced electron transfer from ferrocene to fullerene was identified with lifetimes for the charge-separated state of 560 ns (THF) and 490 ns (benzonitrile). The various properties observed indicate that liquid-crystalline dyads based on ferrocene and fullerene are valuable candidates for the development of supramolecular switches.

Experimental

Materials

All materials were reagent grade chemicals. TBAH (puriss from Fluka) was used as supporting electrolyte as received. CH_2Cl_2 (Fluka) was transferred, under argon, from the original air-tight container into a Schlenk flask containing activated 4 Å molecular sieves and kept under vacuum prior to use. Tetrahydrofuran (THF, LiChrosolv, Merck) was treated according to a procedure described elsewhere.[24] For the electrochemical experiments, the solvent was distilled into the electrochemical cell, prior to use, using a trap-to-trap procedure. [60]Fullerene was purchased from Bucky-USA (99.5%), and all other reagents and solvents were used as purchased from Fluka, Aldrich, J. T. Baker and Cambridge Isotope Laboratories. The silica gel NM Kieselgel 60 (70–230 mesh ASTM) was obtained from Macherey-Nagel and was used as the support for any column chromatographies. Compounds **2**[20] and **3**[21] were prepared as reported in the literature.

Liquid-crystalline and thermal properties

Transition temperatures (onset point) and enthalpies were determined with a differential scanning Mettler DSC 822 calorimeter, under N_2/He, at a rate of 10 °C min^{-1}. Optical studies were conducted using a Zeiss-Axioscope polarizing microscope equipped with a Linkam-THMS-600 variable-temperature stage under N_2. The XRD patterns were obtained with a pinhole camera (Antoon-Paar) operating with a point-focussed Ni-filtered Cu-Kα beam. The samples were held in

Lindemann glass capillaries (1 mm diameter) and heated with a variable-temperature oven. The patterns were collected on flat photographic films. The capillary axis and the film are perpendicular to the X-ray beam. Spacings were obtained *via* Bragg's law.

Electrochemical instrumentation and measurements

The one-compartment electrochemical cell was of airtight design with high-vacuum glass stopcocks fitted with either Teflon or Viton O-rings in order to prevent contamination by grease. The connections to the high-vacuum line and to the Schlenck containing the solvent were obtained by spherical joints also fitted with Viton O-rings. The pressure measured in the electrochemical cell prior to performing the trap-to-trap distillation of the solvent was typically 1.0 to 2.0 $\times$ 10^{-5} mbar. The working electrode was a Pt disc electrode (diameter: 125 μm) sealed in glass. The counter electrode consisted of a platinum spiral and the quasi-reference electrode was a silver spiral. The quasi-reference electrode drift was negligible for the time required by a single experiment. Both the counter and reference electrodes were separated from the working electrode by $\sim$0.5 cm. Potentials were measured with respect to ferrocene standard, and are always referred to saturated calomel electrode (SCE). $E_{1/2}$ values correspond to $(E_{pc} + E_{pa})/2$ from CV. Ferrocene was also used as an internal standard for checking the electrochemical reversibility of a redox couple. Voltammograms were recorded with a AMEL Model 552 potentiostat or a custom made fast potentiostat controlled by either a AMEL Model 568 function generator or a ELCHEMA Model FG-206F. Data acquisition was performed by a Nicolet Model 3091 digital oscilloscope interfaced to a PC. Temperature control was accomplished within 0.1 °C with a Lauda thermostat.

Photophysical instrumentation and measurements

Picosecond laser flash photolysis experiments were carried out with 355 nm laser pulses from a mode-locked, Q-switched Quantel YG-501 DP Nd:YAG laser system (pulse width 18 ps, 2–3 mJ/pulse). The white continuum picosecond probe pulse was generated by passing the fundamental output through a D_2O/H_2O solution. The excitation and the probe was fed to a spectrograph (HR-320, ISDA Instruments, Inc.) with fiber-optic cables and was analyzed with a dual diode array detector (Princeton Instruments, Inc.) interfaced with an IBM-AT computer. The details of the experimental set up and its operation have been described elsewhere.[31]

Nanosecond laser flash photolysis experiments were performed with laser pulses from a Molectron UV-400 nitrogen laser system (337.1 nm, 8 ns pulse width, 1 mJ/pulse). The photomultiplier output was digitized with a Tektronix 7912 AD programmable digitizer. A typical experiment consisted of 5–10 replicate pulses per measurement. The averaged signal was processed with an LSI-11 microprocessor interfaced with a VAX-370 computer. Details of the experimental set up can be found elsewhere.[31] Intersystem crossing rates were determined by averaging the singlet–singlet decay and triplet–triplet growth dynamics.

Time-resolved emission fluorescence lifetimes were measured with a Laser Strobe Fluorescence Lifetime Spectrometer (Photon Technology International) with 337 nm laser pulses from a nitrogen laser fiber-coupled to a lens-based T-formal sample compartment equipped with a stroboscopic detector. Details of the Laser Strobe systems are described on the manufactures web site, http://www.pti-nj.com.

Steady-state emission and excitation spectra were recorded with a SLM 8100 Spectrofluorometer. Fluorescence spectra were measured at room temperature. A 600 nm long-pass filter in the emission path was used to eliminate the interference from the solvent and stray light for recording the fullerene fluorescence, respectively. Fluorescence quantum yields were determined *via* the comparative method, using 9,10-diphenylanthracene as reference with a quantum yield of 1. No corrections were performed for the fluorescence, but long integration times (20 s) and low increments (0.1 nm) were applied. The slits were 2 and 8 nm and each spectrum was an average of at least 5 individual scans.

Synthesis

FT-IR spectra were recorded on Jasco spectrophotometer FT/IR-200 using KBr powder (DRIFT system). UV spectra were recorded on a Perkin Elmer Lambda 20 spectrophotometer. ^{1}H and ^{13}C NMR spectra were recorded on a Varian Gemini-200 spectrometer at 200 and 50 MHz, respectively, with TMS as internal standard. Chemical shifts are given in ppm relative to that of tetramethylsilane. Abbreviations: column chromatography = CC; 1-(3-dimethylaminopropyl)-3-ethylcarbodiimide hydrochloride = EDC; 1-hydroxybenzotriazole = HOBT.

Compound 4

A mixture of C_{60} (39 mg, 0.054 mmol), aldehyde **2** (50 mg, 0.018 mmol) and amino acid **3** (28 mg, 0.092 mmol, solution in 1 mL of methanol) in toluene (55 mL) was heated under reflux for 1 h. After cooling the solution to rt, the product was purified by CC (eluant toluene, then toluene/ethyl acetate 10 : 1) and then precipitated from CH_2Cl_2 solution with methanol. Yield (based on starting aldehyde): 79% (53 mg, 0.014 mmol). ^{1}H NMR ($CDCl_3$): δ = 8.92 (t, J = 1.5 Hz, 1H), 8.62 (t, J = 1.5 Hz, 2H), 8.34 (d, J = 1.5 Hz, 2H), 8.21–8.02 (m, 16H), 7.89 (d, J = 7.5 Hz, 2H), 7.65–7.54 (m, 24), 7.37–7.22 (m, 8H), 7.03–6.89 (m, 10H), 5.21 (s, 1H), 5.19 (d, J = 9.3 Hz, 1H), 4.97 (t, J = 5.2 Hz, 1H), 4.46–4.21 (m, 11H), 4.13–3.91 (m, 12H), 3.83–3.66 (m, 4H), 3.58 (t, J = 5.2 Hz, 2H), 3.46–3.34 (m, 1H), 3.33 (quint, J = 5.2 Hz, 2H), 2.98–2.81 (m, 1H), 1.89–1.68 (m, 20H), 1.55–1.22 (m, 69H). ^{13}C NMR ($CDCl_3$): δ = 166.41, 164.88, 164.45, 164.08, 163.68, 163.08, 156.22, 155.94, 154.00, 152.96, 151.58, 150.53, 147.32, 146.55, 146.30, 145.94, 145.70, 145.55, 145.36, 145.26, 144.85, 144.72, 144.54, 144.42, 143.16, 143.00, 142.70, 142.58, 142.46, 142.15, 142.03, 141.84, 141.53, 140.24, 139.89, 139.47, 136.98, 136.70, 136.43, 135.98, 135.61, 132.69, 132.39, 131.14, 130.67, 129.94, 129.52, 129.17, 128.38, 127.72, 127.08, 122.62, 121.22, 120.33, 118.95, 114.61, 114.41, 111.02, 82.05, 79.27, 76.08, 70.64, 70.50, 69.33, 68.43, 67.77, 65.99, 65.37, 52.27, 40.56, 29.85, 29.57, 29.47, 29.23, 28.78, 28.59, 26.11. IR-DRIFT (KBr): 3427, 2927, 2855, 2226, 1727, 1602, 1252, 1063, 844, 756, 532, 423 cm^{-1}.

Compound 5

Trifluoroacetic acid (1.5 mL) was added to a solution of **4** (78 mg, 0.021 mmol) in CH_2Cl_2 (3 mL). The reaction mixture was stirred at rt for 1 h. After evaporation of solvent, the salt was washed with toluene, dissolved in $CHCl_3$ and precipitated by addition of diethyl ether. Yield: 95% (74 mg, 0.020 mmol). ^{1}H NMR ($CDCl_3$): δ = 8.91 (t, J = 1.5 Hz, 1H), 8.61 (t, J = 1.5 Hz, 2H), 8.33 (d, J = 1.5 Hz, 2H), 8.19–8.02 (m, 16H), 7.86 (d, J = 8 Hz, 2H), 7.77–7.55 (m, 24), 7.37–7.21 (m, 8H), 7.02–6.89 (m, 10H), 5.18 (s, 1H), 5.14 (d, J = 9.3 Hz, 1H), 4.46–4.16 (m, 11H), 4.09–3.92 (m, 12H), 3.86–3.69 (m, 4H), 3.51–3.28 (m, 3H), 3.25–3.07 (m, 2H), 2.92–2.77 (m, 1H), 1.89–1.62 (m, 20H), 1.55–1.20 (m, 60H). IR-DRIFT (KBr): 3063, 2928, 2860, 2225, 1912, 1728, 1602, 1502, 1252, 1064, 1009, 843, 757, 533 cm^{-1}.

Compound 1

A solution of ferrocene carboxylic acid (3.5 mg, 0.015 mmol), EDC (4.4 mg, 0.023 mmol) and HOBT (3.1 mg, 0.023 mmol) in

CH_2Cl_2 (2 mL) was stirred at rt for 15 min, and then added dropwise to a suspension of **5** (28.4 mg, 0.0077 mmol) and Et_3N (2.6 mL, 0.019 mmol) in CH_2Cl_2 (2 mL). The mixture was stirred at rt overnight. The product was purified by CC (toluene/ethyl acetate 85 : 15), and then precipitated from CH_2Cl_2 solution using diethyl ether. Yield: 39% (11.5 mg, 0.0030 mmol). ^{1}H NMR ($CDCl_3$): δ = 8.91 (t, J = 1.5 Hz, 1H), 8.61 (t, J = 1.5 Hz, 2H), 8.33 (d, J = 1.5 Hz, 2H), 8.17–8.01 (m, 16H), 7.87 (d, J = 7.8 Hz, 2H), 7.56–7.54 (m, 24H), 7.34–7.20 (m, 8H), 7.02–6.87 (m, 10H), 6.18 (t, J = 5.0 Hz, 1H), 5.18 (s, 1H), 5.17 (d, J = 9.1 Hz, 1H), 4.67–4.16 (m, 2H), 4.40–4.20 (m, 13H), 4.18 (s, 5H), 4.06–3.94 (m, 12H), 3.84–3.72 (m, 4H), 3.67 (q, J = 5.0 Hz, 2H), 3.59 (quint, J = 5.0 Hz, 2H), 3.45–3.29 (m, 1H), 2.94–2.78 (m, 1H), 1.87–1.65 (m, 20H), 1.51–1.20 (m, 60H). ^{13}C ($CDCl_3$): δ = 164.79, 164.30, 164.01, 162.99, 151.52, 150.48, 146.23, 145.29, 144.80, 142.53, 136.64, 132.60, 132.30, 131.08, 129.86, 129.43, 129.04, 128.28, 127.64, 126.97, 122.52, 121.16, 118.83, 114.51, 114.34, 110.99, 70.42, 69.84, 68.37, 65.89, 29.51, 29.38, 29.28, 29.14, 28.70, 26.03. IR-DRIFT (KBr): 3075, 2926, 2225, 1727, 1601, 1252, 1063, 842, 756, 526 cm^{-1}. Vis (λ_{max}/nm (ε/dm^3 $mol^{-1}cm^{-1}$), CH_2Cl_2): 431 (4090), 701 (360).

Acknowledgements

This work was supported by the Office of Basic Energy Sciences of the US Department of Energy (NDRL-4517), the University of Trieste, EU (RTN program "WONDERFULL"), MIUR (PRIN 2002, prot. 2002032171), and the University of Bologna (Funds for Selected Research Topics), MIUR (PRIN 2002035735). RD acknowledges the Swiss National Science Foundation (grants no 2000-058956.99 and 2000-066721.01) and the Swiss Federal Office for Education and Science (grant no 01.0377, RTN Project "Fullerene-based Advanced Materials for Optoelectronic Utilizations" (FAMOUS) from the European Union (HPRN-CT-2002-00171)) for financial support.

References

1 D. M. Guldi and M. Prato, *Acc. Chem. Res.*, 2000, **33**, 695.
2 N. Martín, L. Sánchez, B. Illescas and I. Pérez, *Chem. Rev.*, 1998, **98**, 2527.
3 H. Imahori and Y. Sakata, *Eur. J. Org. Chem.*, 1999, 2445.
4 D. M. Guldi, *Chem. Commun.*, 2000, 321.
5 D. M. Guldi, *Chem. Soc. Rev.*, 2002, **31**, 22.
6 D. Carbonera, M. Di Valentin, C. Corvaja, G. Agostini, G. Giacometti, P. A. Liddell, D. Kuciauskas, A. L. Moore, T. A. Moore and D. Gust, *J. Am. Chem. Soc.*, 1998, **120**, 4398.
7 J.-F. Nierengarten, J.-F. Eckert, J.-F. Nicoud, L. Ouali, V. Krasnikov and G. Hadziioannou, *Chem. Commun.*, 1999, 617.
8 J.-F. Eckert, J.-F. Nicoud, J.-F. Nierengarten, S.-G. Liu, L. Echegoyen, F. Barigelletti, N. Armaroli, L. Ouali, V. Krasnikov and G. Hadziioannou, *J. Am. Chem. Soc.*, 2000, **122**, 7467.
9 E. Peeters, P. A. van Hal, J. Knol, C. J. Brabec, N. S. Sariciftci, J. C. Hummelen and R. A. J. Janssen, *J. Phys. Chem. B*, 2000, **104**, 10174.
10 A. Marcos Ramos, M. T. Rispens, J. K. J. van Duren, J. C. Hummelen and R. A. J. Janssen, *J. Am. Chem. Soc.*, 2001, **123**, 6714.
11 C. J. Brabec, N. S. Sariciftci and J. C. Hummelen, *Adv. Funct. Mater.*, 2001, **11**, 15.
12 A. Cravino, G. Zerza, M. Maggini, S. Bucella, M. Svensson, M. R. Andersson, H. Neugebauer and N. S. Sariciftci, *Chem. Commun.*, 2000, 2487.
13 A. Cravino, G. Zerza, H. Neugebauer, M. Maggini, S. Bucella, E. Menna, M. Svensson, M. R. Andersson, C. J. Brabec and N. S. Sariciftci, *J. Phys. Chem. B*, 2002, **106**, 70.
14 D. Gust, T. A. Moore and A. L. Moore, *Acc. Chem. Res.*, 2001, **34**, 40.
15 D. M. Guldi, M. Maggini, G. Scorrano and M. Prato, *J. Am. Chem. Soc.*, 1997, **119**, 974.
16 R. Deschenaux, M. Even and D. Guillon, *Chem. Commun.*, 1998, 537.
17 M. Even, B. Heinrich, D. Guillon, D. M. Guldi, M. Prato and R. Deschenaux, *Chem. Eur. J.*, 2001, **7**, 2595.
18 C. Bingel, *Chem. Ber.*, 1993, **126**, 1957.
19 J.-P. Bourgeois, F. Diederich, L. Echegoyen and J.-F. Nierengarten, *Helv. Chim. Acta*, 1998, **81**, 1835.
20 S. Campidelli and R. Deschenaux, *Helv. Chim. Acta*, 2001, **84**, 589.
21 K. Kordatos, T. Da Ros, S. Bosi, E. Vásquez, M. Bergamin, C. Cusan, F. Pellarini, V. Tomberli, B. Baiti, D. Pantarotto, V. Georgakilas, G. Spalluto and M. Prato, *J. Org. Chem.*, 2001, **66**, 4915.
22 T. Chuard and R. Deschenaux, *J. Mater. Chem.*, 2002, **12**, 1944.
23 B. Dardel, D. Guillon, B. Heinrich and R. Deschenaux, *J. Mater. Chem.*, 2001, **11**, 2814.
24 F. Paolucci, M. Carano, P. Ceroni, L. Mottier and S. Roffia, *J. Electrochem. Soc.*, 1999, **146**, 3357.
25 S. Cattarin, P. Ceroni, D. M. Guldi, M. Maggini, E. Menna, F. Paolucci, S. Roffia and G. Scorrano, *J. Mater. Chem.*, 1999, **9**, 2743.
26 T. Da Ros, M. Prato, M. Carano, P. Ceroni, F. Paolucci and S. Roffia, *J. Am. Chem. Soc.*, 1998, **120**, 11645.
27 For peaks I–IV in the CV curve of Fig. 3c, a four (unequal) step sigmoidal curve is obtained after convolution, where each step is proportional to n of the corresponding CV peak: A. J. Bard and L. R. Faulkner, *Electrochemical Methods. Fundamentals and Applications*, Wiley, New York, 2000.
28 A similar trend was seen in a fullerene–ferrocene reference dyad, which lacks the mesogenic unit, confirming that the latter has no meaningful impact on the fullerene singlet excited state deactivation.
29 D. M. Guldi, M. Maggini, G. Scorrano and M. Prato, *Res. Chem. Intermed.*, 1997, **23**, 561.
30 D. M. Guldi, C. Luo, N. A. Kotov, T. Da Ros, S. Bosi and M. Prato, *J. Phys. Chem. B*, 2003, **107**, 7293.
31 M. D. Thomas and G. L. Hug, *Comput. Chem.*, 1998, **22**, 491.